Supporting Information

Pore-Wall Pyridine-N Density Regulation in Covalent Organic Frameworks for Enhanced Gold Capture

Jun Cao, Meng Li, Hao Wang, Shiyuan Wei, Ruoyan Li, Jinping Xiahou, Jianhan Huang*, Jiawei Li*, and You-Nian Liu

Experimental Section

Materials and reagents

1,3,6,8-Tetra(4-aminophenyl)pyrene (PYTA) (Cat No. 1181502, Leyan, Shanghai, China) and chloroauric acid trihydrate ($HAuCl_4 \cdot 3H_2O$) (Cat No. 1215225, Leyan, Shanghai, China). Terephthalaldehyde (PT), styrene (St), 2-vinylpyridine (2-VPy), and 2-vinylpyrazine (2-VPz) were obtained from Aladdin. *n*-Butanol (*n*-BuOH), *o*-dichlorobenzene (*o*-DCB), dichloromethane (DCM), tetrahydrofuran (THF), methanol (MeOH), acetic acid (HAc), and sodium hydroxide (NaOH) were purchased from Sinopharm Chemical Reagent Co., Ltd. 2,3-Dichloro-5,6-dicyano-1,4-benzoquinone (DDQ) and boron trifluoride diethyl etherate ($BF_3 \cdot Et_2O$) were obtained from Adamas. All other reagents and solvents were purchased from commercial sources and used as received without further purification.

Characterization

Scanning electron microscopy (SEM) images were acquired on a JSM-7610F Plus microscope at an accelerating voltage of 10 kV. Transmission electron microscopy (TEM) was performed on a JEM-F200 instrument operated at 120 kV. Thermogravimetric analysis (TGA) was carried out on a Mettler Toledo TGA2 under a N_2 atmosphere from 25 to 800 °C at a heating rate of 10 °C min^{-1}. Powder X-ray diffraction (PXRD) patterns were collected on a Bruker D8 Advance diffractometer using Ni-filtered Cu Kα radiation (40 kV, 100 mA) over the 2θ range of 2-30° at a scanning rate of 6° min^{-1}. Fourier transform infrared (FT-IR) spectra were recorded on a Nicolet iN10 MX microscope FT-IR spectrometer in the range of 4000-500 cm^{-1}. N_2 adsorption-desorption isotherms at 77 K were measured on a Micromeritics ASAP 2460 analyzer to evaluate the porosity and textural properties. X-ray photoelectron spectroscopy (XPS) measurements were carried out on an ESCALAB Xi+ spectrometer equipped with an Al Kα X-ray source. Solid-state ^{13}C NMR spectra were recorded on a Bruker Avance II 400 MHz spectrometer with a contact time of 2 ms (ramp 100%)

and a recycle delay of 4 s. Metal-ion concentrations were determined using a TAS-990 atomic absorption spectrometer (AAS).

Synthesis

Synthesis of Model Compound

A Pyrex glass tube (10 mL) was charged with benzaldehyde (69 mg, 0.65 mmol), aniline (60 mg, 0.65 mmol), styrene (0.68 mmol, 78 μL), 2,3-dichloro-5,6-dicyano-1,4-benzoquinone (DDQ) (5.2 mg, 0.02 mmol), and $BF_3 \cdot Et_2O$ (4 μL, 0.03 mmol) in o-dichlorobenzene (o-DCB)/n-BuOH (1.5/1.5 mL). The tube was firstsonicated for 30 minutes to form bulk solid and then flash frozen at 77 K (liquid N_2 bath) and degassed by three times of freeze-pump-thaw cycles. The internal pressurewas evacuated to 10^{-3} mbar. The tube was sealed and heated at 120 °C for 1 days. The resulting crystalline solid was collected by filtration, gently washed with THF and MeOH, and dried under vacuum to afford the desired quinoline product in 80% isolated yield

Synthesis of COF-Q-Ph

PYTA (33.9 mg, 0.06 mmol, 1.0 eq) and PT (16.1 mg, 0.12 mmol, 2.0 eq) were placed in a 10 mL Pyrex tube, followed by addition of a solvent mixture of *o*-dichlorobenzene/*n*-butanol (*o*-DCB/*n*-BuOH, 1:1, v/v; total 3.0 mL). Acetic acid (6 M, 0.30 mL) was then added, and the mixture was sonicated for 5 min until a homogeneous solution was obtained. Subsequently, St (25.0 mg, 0.24 mmol, 4.0 eq), DDQ (3.63 mg, 0.016 mmol, 0.27 eq), and $BF_3 \cdot Et_2O$ (6 μL, 0.048 mmol, 0.80 eq) were added. The reaction mixture was degassed by three freeze-pump-thaw cycles, flame-sealed under vacuum, and heated at 120 °C for 72 h. After cooling to room temperature, the resulting solid was collected and washed with THF and MeOH. Further purification of the product was carried out using a Soxhlet extractor with THF and methanol for 24 h. Finally, the product was dried under vacuum at 60 °C for 24 h.

Synthesis of COF-Q-Py and COF-Q-Pz

COF-Q-Py and COF-Q-Pz were prepared under identical conditions, except that styrene was replaced with 2-VPy (25.23 mg, 0.24 mmol, 4.0 eq) for COF-Q-Py or 2-VPz (25.47 mg, 0.24 mmol, 4.0 eq) for COF-Q-Pz.

Adsorption isotherm

For adsorption isotherm experiments, $AuCl_4^-$ solutions were prepared from $HAuCl_4 \cdot 3H_2O$ with initial concentrations of 100, 200, 300, 400, and 500 mg L^{-1}. Typically, 3.0 mg of COF was added to 15.0 mL of $AuCl_4^-$ solution and stirred at room temperature for 12 h to reach adsorption equilibrium. After filtration through a 0.22 μm membrane, the equilibrium $AuCl_4^-$ concentration (C_e) in the filtrate was determined by AAS (TAS-990). The solution pH was not adjusted unless otherwise noted. The equilibrium adsorption capacity (q_e, mg g^{-1}) was calculated according to Eq. (1):

$$q_e = \frac{(C_0 - C_e)V}{m} \tag{1}$$

where C_0 (mg/L) and C_e (mg/L) are the initial and equilibrium concentrations of $AuCl_4^-$, respectively, V (L) is the solution volume (15.0 mL), and m (g) is the mass of the adsorbent. The isotherm data were fitted using the Langmuir model (Eq. (2)) and the Freundlich model (Eq. (3)):

$$q_e = \frac{K_L q_m C_e}{1 + K_L C_e} \tag{2}$$

$$q_e = K_F C_e^{\frac{1}{n}} \tag{3}$$

where q_m (mg g^{-1}) is the maximum adsorption capacity, K_L (L mg^{-1}) is the Langmuir constant, K_F is the Freundlich constant, and n is the heterogeneity factor.

Adsorption kinetics

For kinetic experiments, 9.0 mg of COF was added to 45.0 mL of $AuCl_4^-$ solution prepared from $HAuCl_4 \cdot 3H_2O$ (250 mg L^{-1}). At predetermined time intervals (10, 20, 30, 40, 50, 60, 90, 120, and 180 min), aliquots were withdrawn and immediately filtered through a 0.22 μm membrane. The $AuCl_4^-$ concentration in the filtrate was determined by AAS (TAS-990). The kinetic data were fitted by nonlinear regression using the pseudo-first-order (PFO) model (Eq. 4) and pseudo-second-order (PSO) model (Eq. 5):

$$q_t = q_e(1 - e^{-k_1 t}) \quad (4)$$

$$q_t = \frac{k_2 q_e^2 t}{1 + k_2 q_e t} \quad (5)$$

where q_t (mg g^{-1}) is the adsorption capacity at time t, q_e (mg g^{-1}) is the equilibrium adsorption capacity, and k_1 (min^{-1}) and k_2 (g mg^{-1} min^{-1}) are the rate constants of the PFO and PSO models, respectively.

Sorption thermodynamics study

Sorption thermodynamic experiments were carried out for COF-Q-Ph, COF-Q-Py, and COF-Q-Pz. $AuCl_4^-$ solutions were prepared from $HAuCl_4 \cdot 3H_2O$ with an initial concentration of 250 mg L^{-1}. Typically, 3.0 mg of COF was added to 15.0 mL of $AuCl_4^-$ solution and mixed at 298, 308, and 318 K for 2 h, respectively. After filtration through a 0.22 μm membrane, the equilibrium $AuCl_4^-$ concentration C_e in the filtrate was determined by AAS (TAS-990). The equilibrium adsorption capacity q_e was calculated as described above. The apparent thermodynamic adsorption equilibrium constant K_e was calculated according to Eq. (6), and the thermodynamic parameters including Gibbs free energy change ΔG, enthalpy change ΔH, and entropy change ΔS were obtained using Eqs. (7) and (8).

$$K_e = \frac{q_e}{C_e} \quad (6)$$

$$\Delta G = -RTInK_e \quad (7)$$

$$InK_e = \frac{\Delta S}{R} - \frac{\Delta H}{RT} \quad (8)$$

where q_e is the equilibrium adsorption capacity in mg g^{-1}, C_e is the equilibrium concentration of $AuCl_4^-$ in mg L^{-1}, K_e is the apparent equilibrium constant in L g^{-1}, T is the absolute temperature in K, and R is the gas constant 8.314 J mol^{-1} K^{-1}. ΔH and ΔS were derived from the slope and intercept of the van't Hoff plot of ln K_e versus 1/T, respectively.

Selectivity tests

Test 1 (Anion interference): An aqueous solution containing Na_2SO_4, NaCl, Na_2CO_3, $NaNO_3$, NaOAc, and Na_3PO_4 was prepared, where the concentration of each

anion salt was 250 ppm. $AuCl_4^-$ was introduced into the same solution at 250 ppm. Typically, 3 mg of the sample was added to 15.0 mL of the above solution and stirred at 25 °C. After the reaction, the suspension was filtered through a 0.22 μm syringe filter, and the residual Au concentration in the filtrate was determined by atomic absorption spectrophotometry (AAS).

Test 2 (Cation interference): A mixed-ion solution containing Na^+, K^+, Zn^{2+}, Pb^{2+}, Ca^{2+}, Cu^{2+}, Al^{3+}, Mg^{2+}, Fe^{3+}, and $AuCl_4^-$ was prepared with a concentration of 250 ppm for each ion species. The sorption procedure and Au analysis were identical to those in Test 1.

Preparation of CPU leaching solution

Discarded central processing units (CPUs) were immersed in 20 mL of aqua regia for 48 h to obtain the initial leachate. The leachate was then adjusted to pH 2.4 and filtered through a 0.22 μm syringe filter to afford the final CPU leaching solution used for subsequent experiments.

Recycling experiments

The recyclability of the sample was evaluated by successive adsorption-desorption cycles. Typically, 20 mg of COF-Q-Pz was added to 40 mL of $AuCl_4^-$ solution (250 ppm) and stirred at room temperature for 2 h. The solid was collected by filtration and washed with water three times. The adsorbed Au species were then eluted by soaking the solid in a regeneration solution containing thiourea (0.01 mol L^{-1}) and HCl (0.05 mol L^{-1}) for 12 h. After regeneration, the material was filtered and washed with water three times, and then reused for the next cycle under identical conditions.

Theoretical calculation

All structural optimizations and subsequent calculations were performed using periodic density functional theory (DFT) as implemented in the CP2K 2024.3 software package.

The bulk structure of the covalent organic framework (COF) was first fully relaxed. The (001) surface was then cleaved to construct a periodic slab model, with a

vacuum layer of 15 Å added along the z-direction to minimize interactions between periodic images in neighboring cells.

Adsorption sites for the reactant(s) on the COF (001) surface were systematically screened across various possible binding positions. The most favorable adsorption configurations were identified based on the computed adsorption energies.

The adsorption energy was calculated using the formula:

$$E_{ads} = E_{AB} - E_A - E_B$$

Where E_{AB} is the total energy of the adsorbate–substrate complex, E_A is the energy of the clean COF slab, and E_B is the energy of the adsorbate in the gas phase.

The computational settings were as follows: the revPBE generalized gradient approximation (GGA) functional was employed to describe electron exchange and correlation. Goedecker–Teter–Hutter (GTH) pseudopotentials were used together with the DZVP-MOLOPT-SR-GTH double-ζ valence plus polarization basis set. Dispersion corrections were included via the DFT-D3 method (Grimme's D3 scheme with zero damping). The orbital transformation (OT) minimizer was adopted for improved SCF convergence during geometry optimizations. The value of cutoff and rel_cutoff was set to 500 Ry and 50 Ry, respectively.

Harmonic vibrational frequencies were computed on the optimized geometries to obtain ZPE corrections and vibrational entropies for free-energy evaluations. Gibbs free energies were computed using the Shermo program.

Post-processing analyses of the electronic structure were carried out with Multiwfn version 3.8. This included calculation of the total and partial density of states (DOS), charge density difference distributions, and atomic charge analysis employing the CM5 charge model. Visualization of the crystal structures and isosurface representations of the charge density difference as well as DOS-projected quantities were performed using the VESTA software.

Supporting Figures and Tables

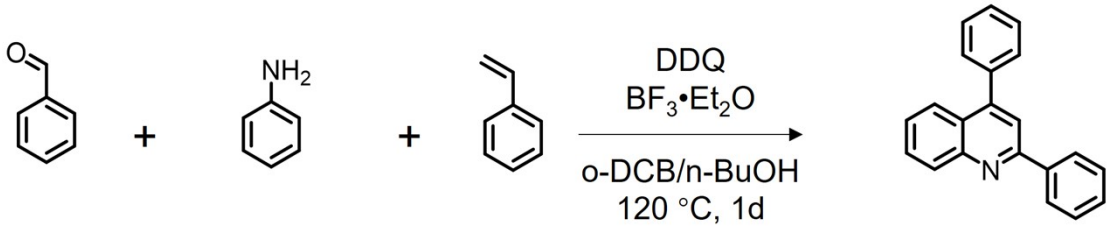

Scheme S1. Synthesis of the model compound.

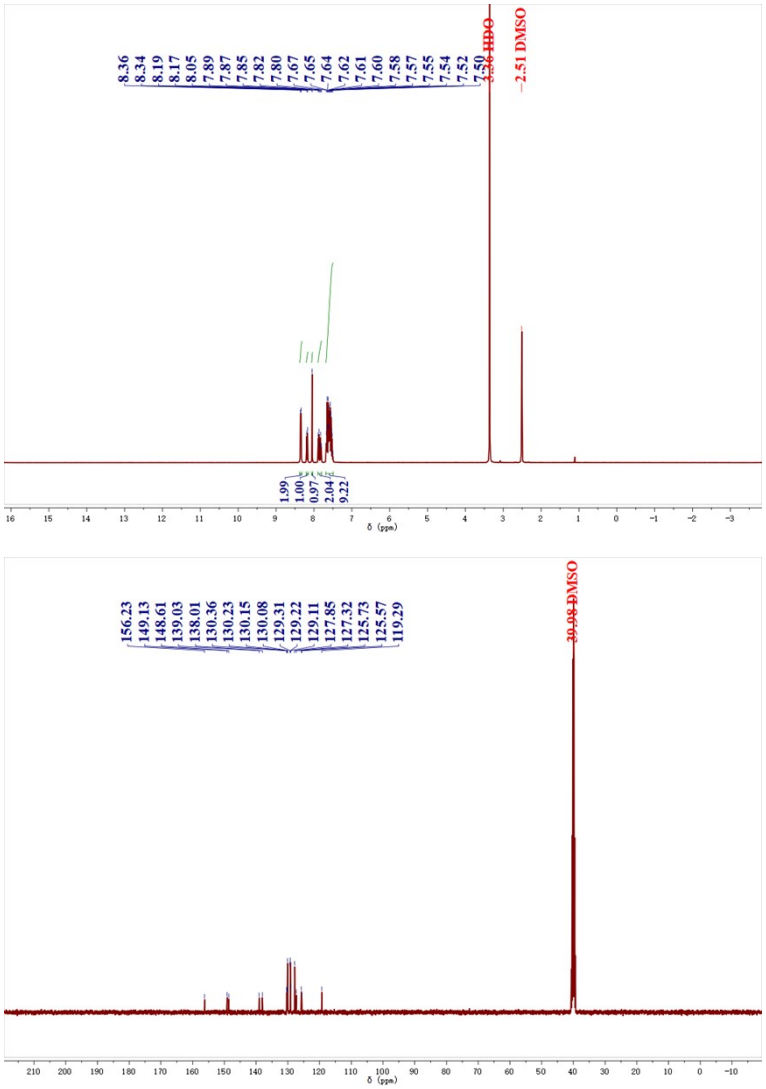

Fig. S1. ^{1}H-NMR (top) and ^{13}C-NMR (bottom) spectra of the model compound performed in DMSO-*d6*.

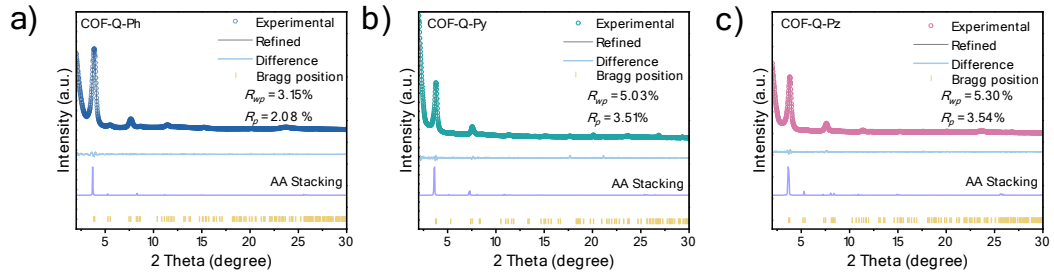

Fig. S2. Experimental and Pawley-refined PXRD patterns of (a) COF-Q-Ph, (b) COF-Q-Py, and (c) COF-Q-Pz.

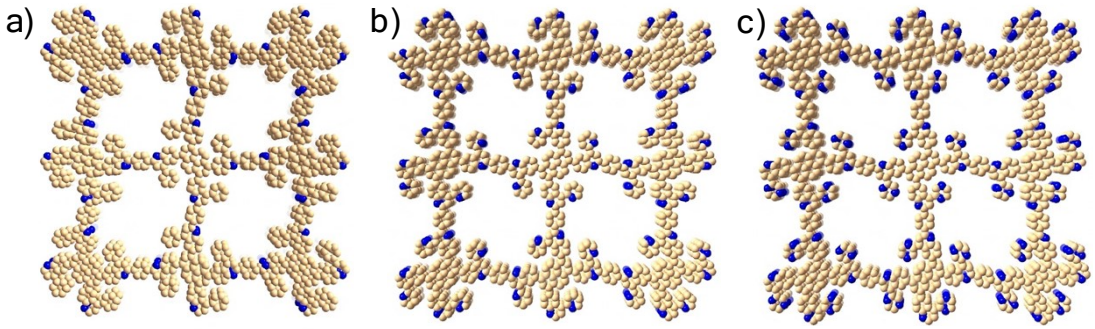

Fig. S3. AA stacking model of (a) COF-Q-Ph, (b) COF-Q-Py, and (c) COF-Q-Pz.

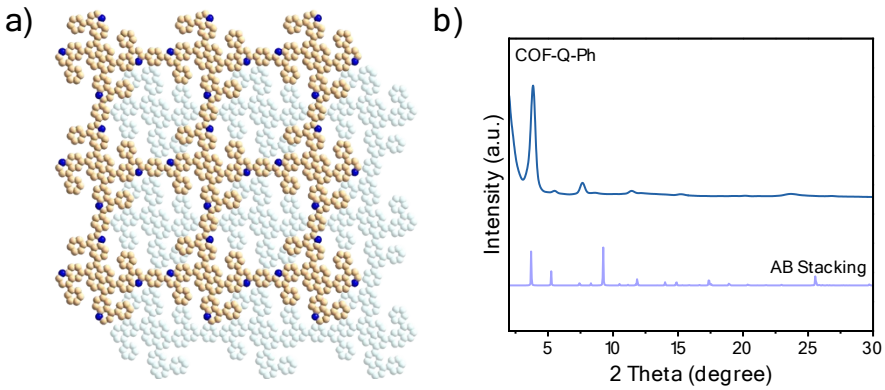

Fig. S4. (a) AB stacking model of COF-Q-Ph and the experimental and simulated (b) PXRD patterns.

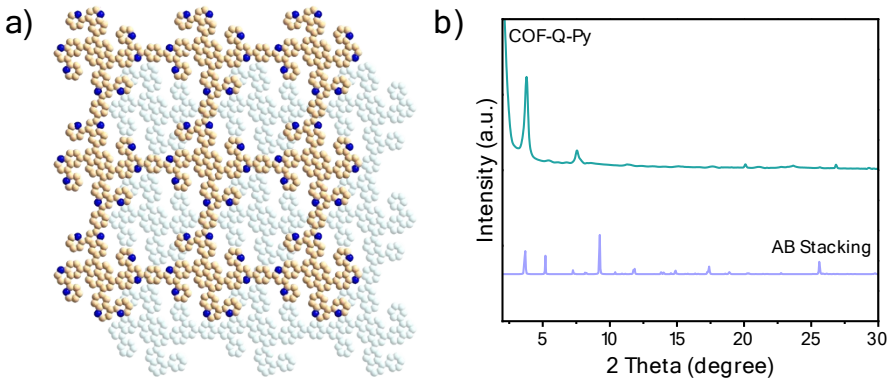

Fig. S5. (a) AB stacking model of COF-Q-Py and the experimental and simulated (b) PXRD patterns.

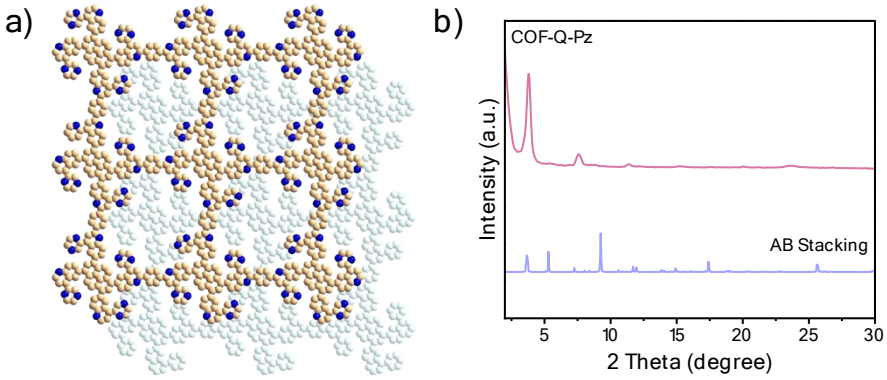

Fig. S6. (a) AB stacking model of COF-Q-Pz and the experimental and simulated (b) PXRD patterns.

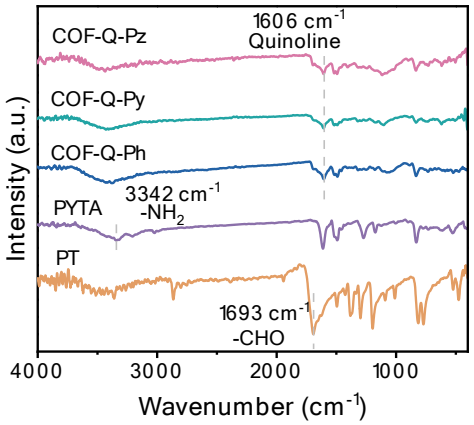

Fig. S7. FT-IR spectra of PT, PYTA, COF-Q-Ph, COF-Q-Py, and COF-Q-Pz.

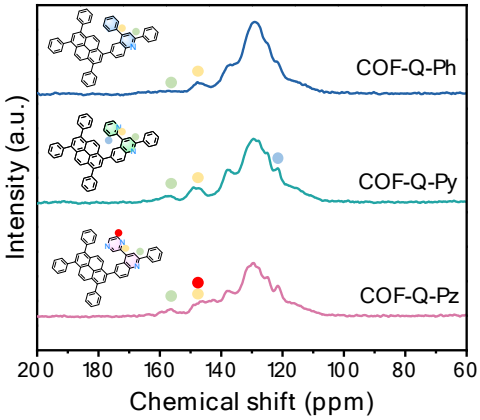

Fig. S8. Solid-state ^{13}C CP/MAS NMR spectra of COF-Q-Ph, COF-Q-Py, and COF-Q-Pz.

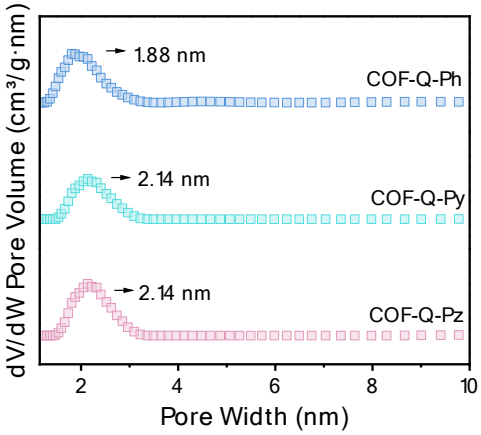

Fig. S9. Pore size distributions of COF-Q-Ph, COF-Q-Py, and COF-Q-Pz.

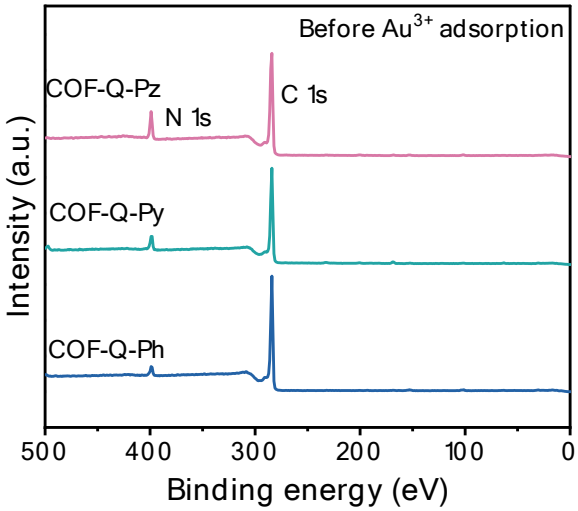

Fig. S10. XPS survey spectra of the COFs before $AuCl_4^-$ adsorption.

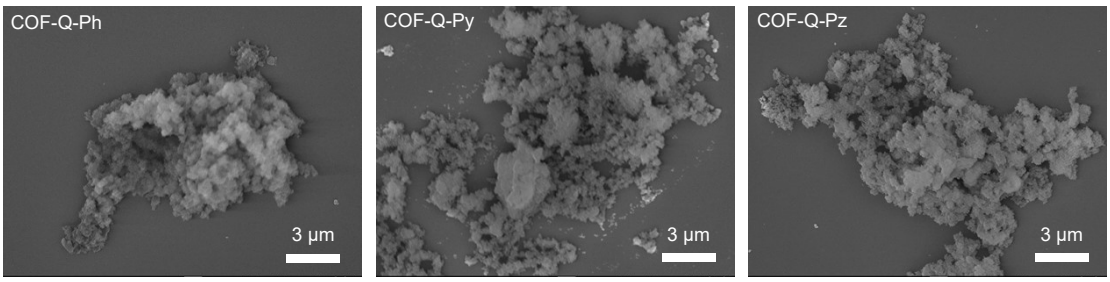

Fig. S11. FE-SEM images of COF-Q-Ph, COF-Q-Py, and COF-Q-Pz.

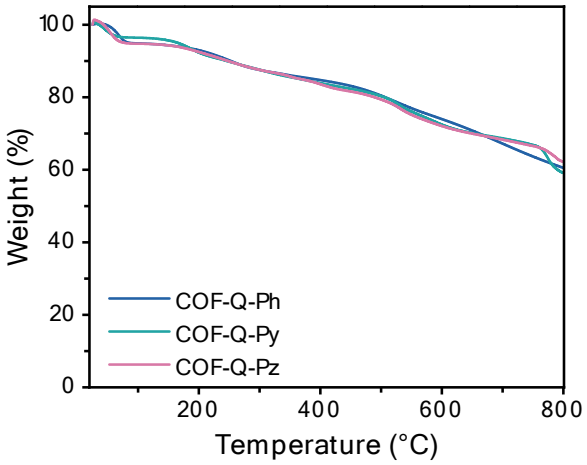

Fig. S12. TGA curves of COF-Q-Ph, COF-Q-Py and COF-Q-Pz under N_2 atmosphere.

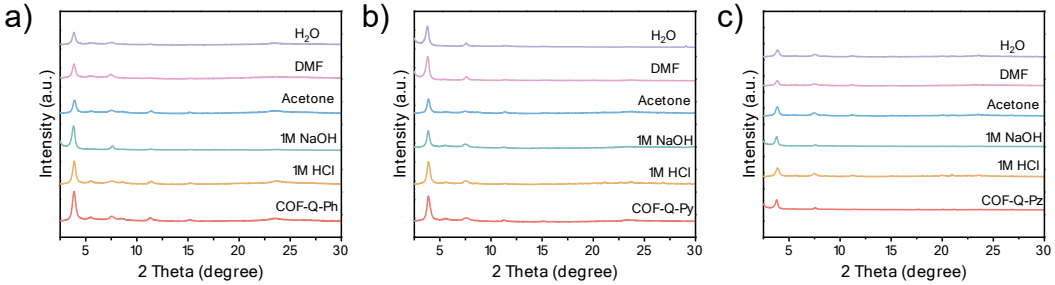

Fig. S13. PXRD after different treatments of (a) COF-Q-Ph, (b) COF-Q-Py, and (c) COF-Q-Pz.

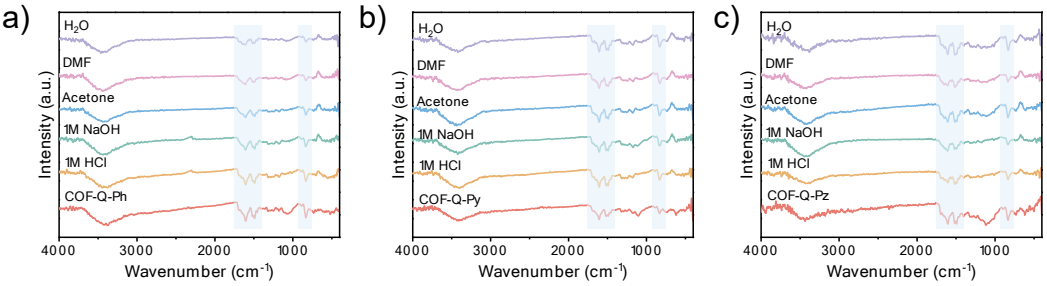

Fig. S14. FT-IR spectra of (a) COF-Q-Ph, (b) COF-Q-Py, and (c) COF-Q-Pz after treatment in various conditions.

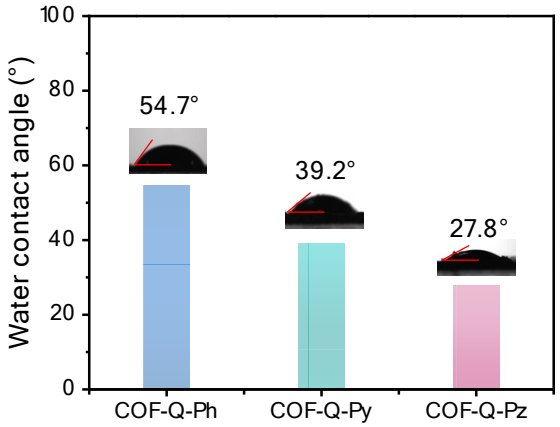

Fig. S15. Water contact angles of COF-Q-Ph, COF-Q-Py, and COF-Q-Pz.

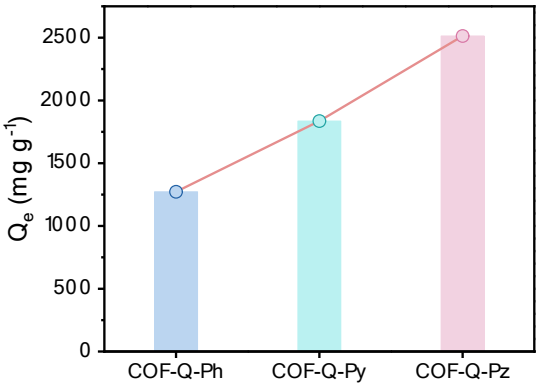

Fig. S16. Comparison of the maximum $AuCl_4^-$ adsorption capacities for COF-Q-Ph, COF-Q-Py, and COF-Q-Pz.

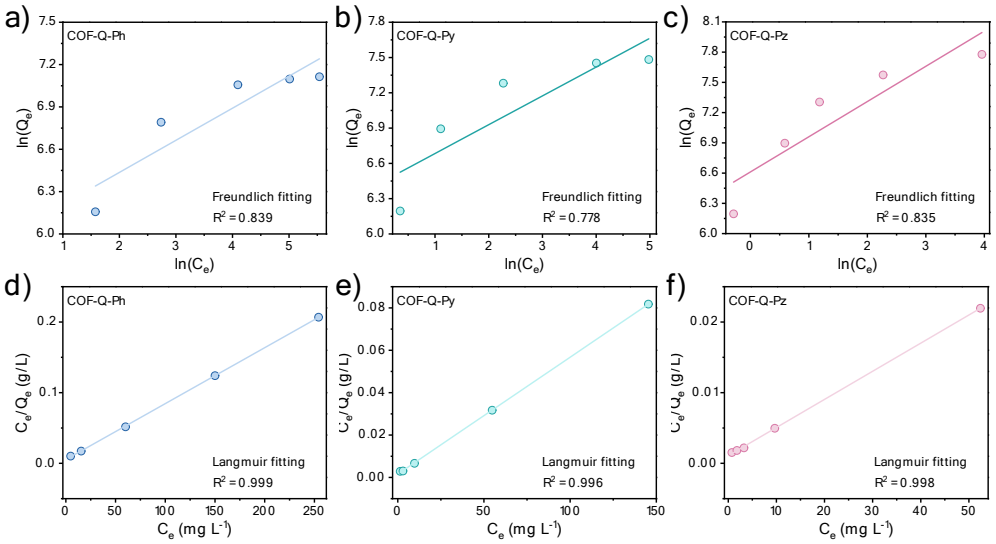

Fig. S17. (a-c) Freundlich and (d-f) Langmuir adsorption isotherm fitting of $AuCl_4^-$ on COF-Q-Ph, COF-Q-Py and COF-Q-Pz.

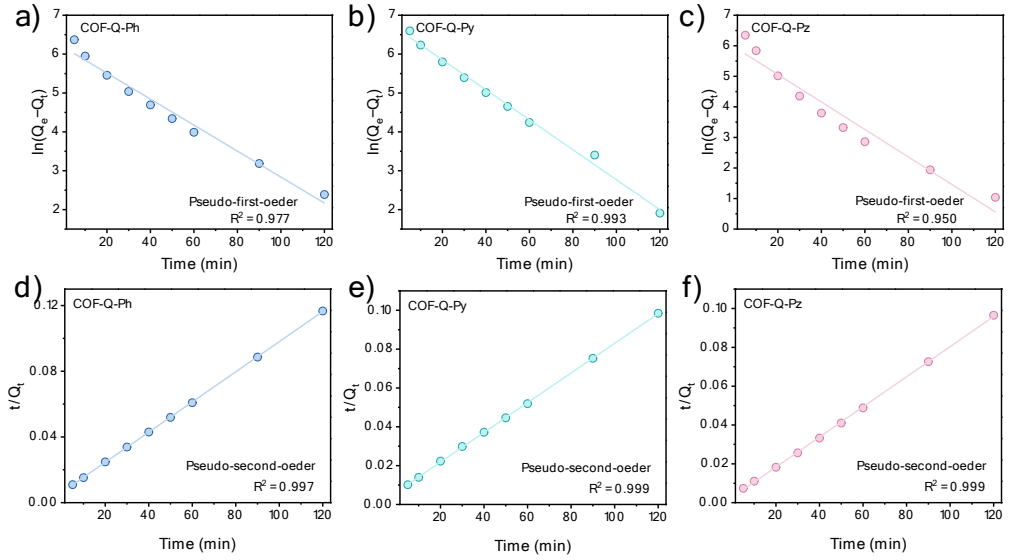

Fig. S18. (a-c) Pseudo-first-order and (d-f) Pseudo-second-order $AuCl_4^-$ adsorption kinetic plots of COF-Q-Ph, COF-Q-Py and COF-Q-Pz.

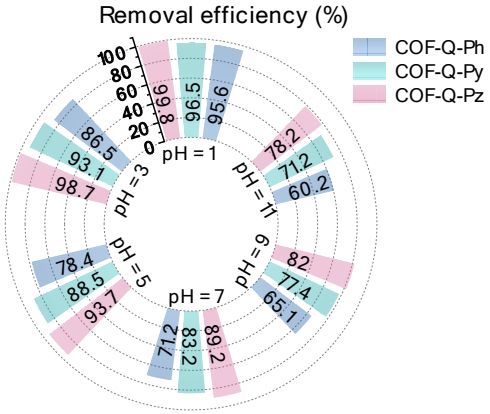

Fig. S19. $AuCl_4^-$ removal efficiencies of COF-Q-Ph, COF-Q-Py and COF-Q-Pz at different pH values.

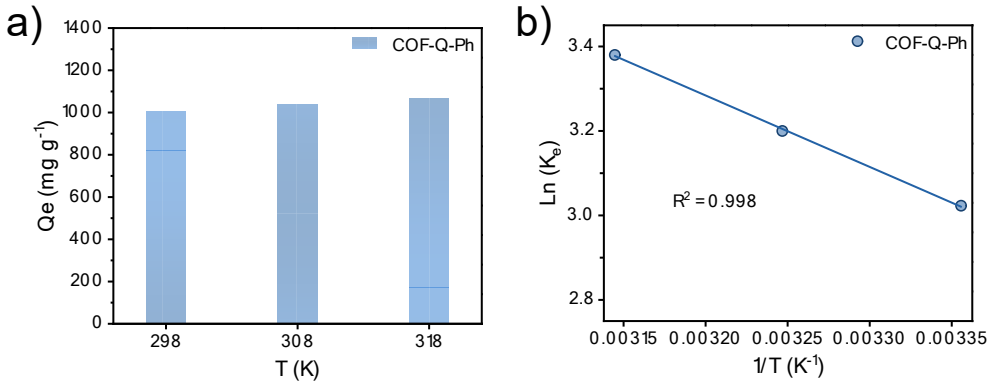

Fig. S20. (a) The adsorption amount of $AuCl_4^-$ of COF-Q-Ph at different temperatures and (b) the corresponding linear fitting model.

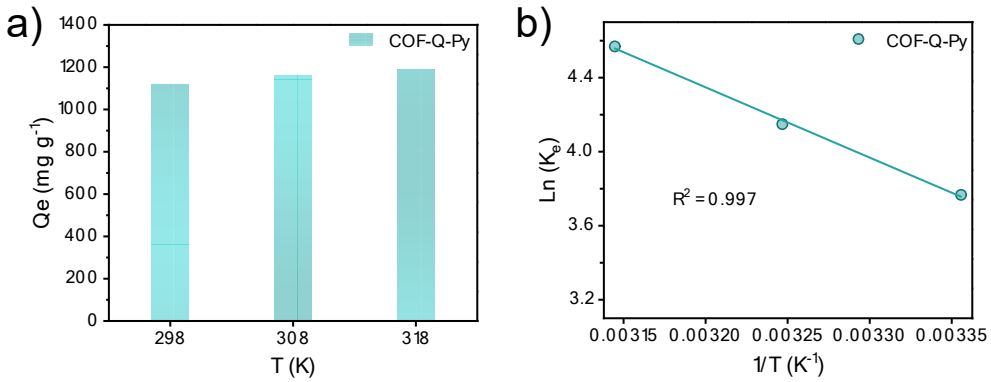

Fig. S21. (a) The adsorption amount of $AuCl_4^-$ of COF-Q-Py at different temperatures and (b) the corresponding linear fitting model.

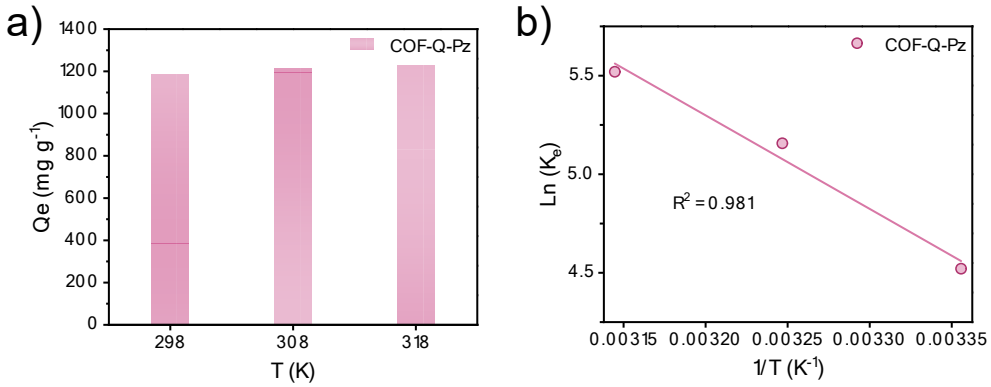

Fig. S22. (a) The adsorption amount of $AuCl_4^-$ of COF-Q-Pz at different temperatures and (b) the corresponding linear fitting model.

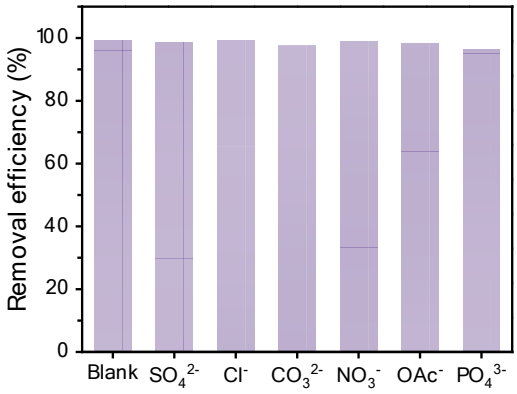

Fig. S23. $AuCl_4^-$ removal efficiencies of COF-Q-Pz in the presence of various competing anions.

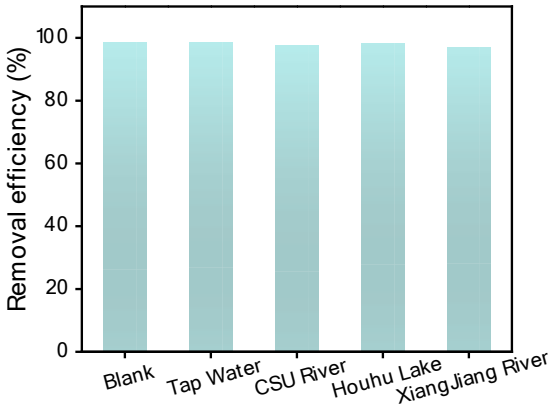

Fig. S24. Recovery of $AuCl_4^-$ by COF-Q-Pz from tap water, CSU River, Houhu Lake and Xiangjiang River.

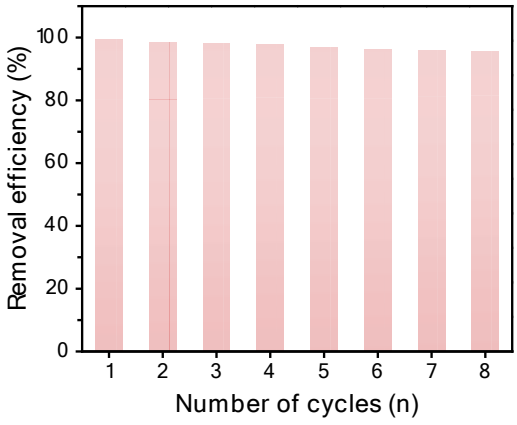

Fig. S25. $AuCl_4^-$ removal efficiencies of COF-Q-Pz over eight adsorption-desorption cycles.

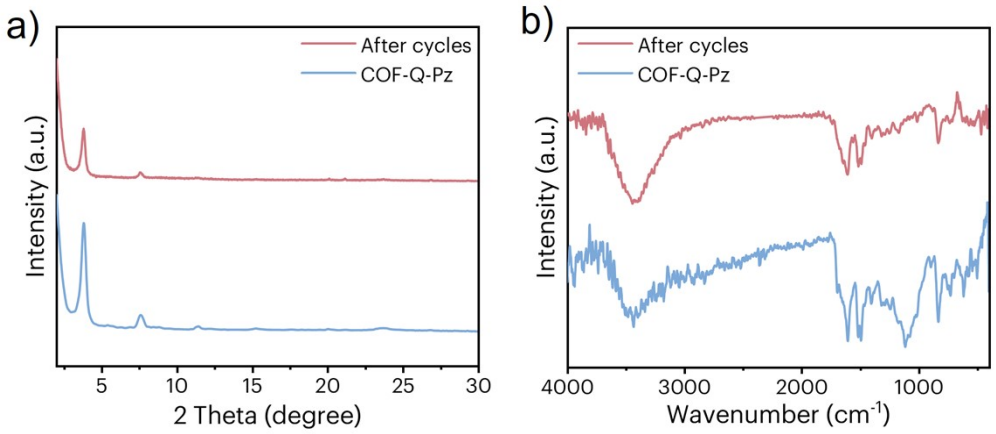

Fig. S26. (a) PXRD patterns and (b) FT-IR spectra of COF-Q-Pz before and after repeated adsorption-desorption cycles.

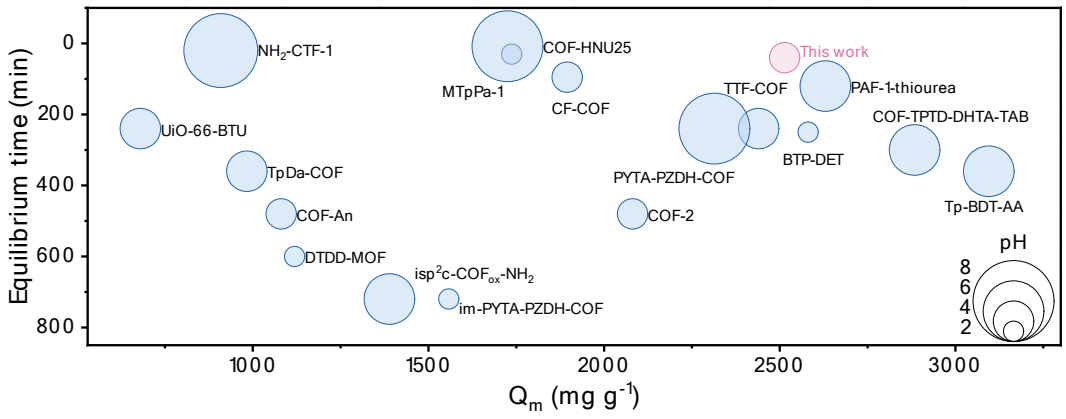

Fig. S27. Comparison of the adsorption capacity and equilibrium time of COF-Q-Pz with previously reported porous adsorbents for $AuCl_4^-$ capture.

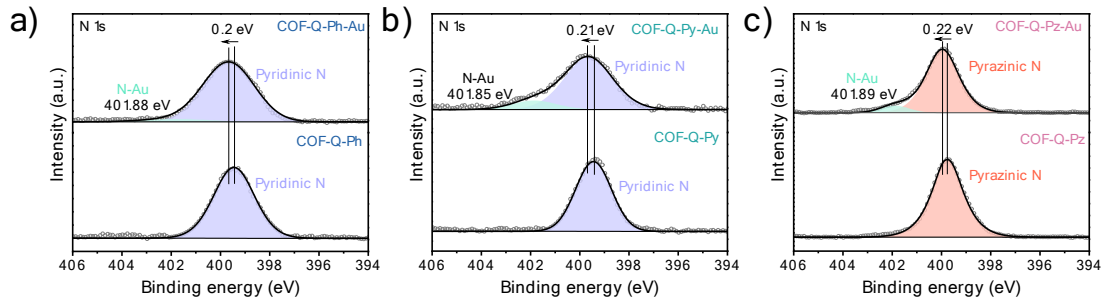

Fig. S28. N 1s XPS spectra of COF-Q-Ph, COF-Q-Py and COF-Q-Pz before and after $AuCl_4^-$ adsorption.

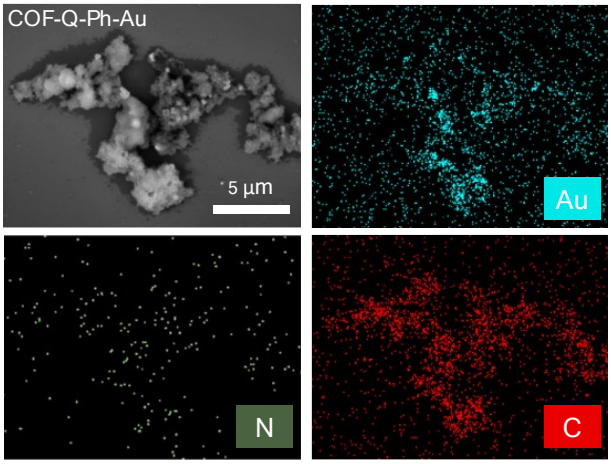

Fig. S29. SEM image and the corresponding EDS mapping of COF-Q-Ph after $AuCl_4^-$ adsorption.

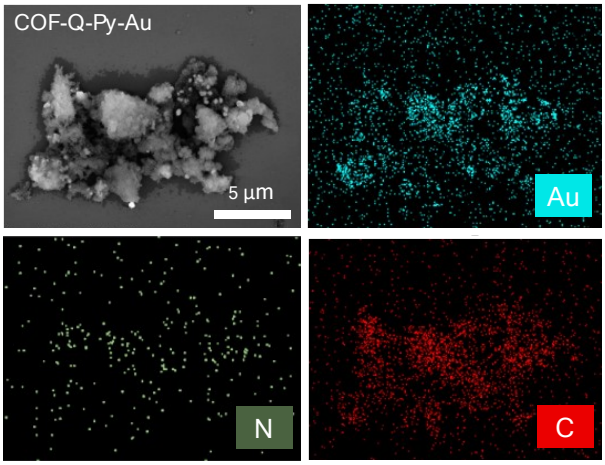

Fig. S30. SEM image and the corresponding EDS mapping of COF-Q-Py after $AuCl_4^-$ adsorption.

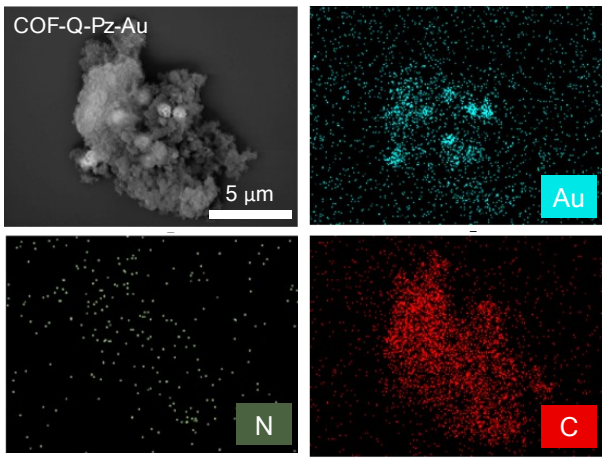

Fig. S31. SEM image and the corresponding EDS mapping of COF-Q-Pz after $AuCl_4^-$ adsorption.

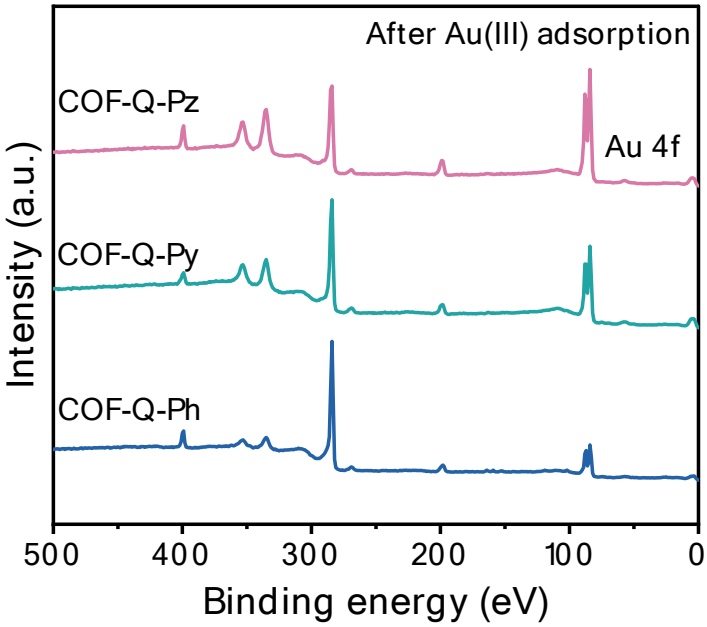

Fig. S32. XPS survey spectra of the COFs after $AuCl_4^-$ adsorption.

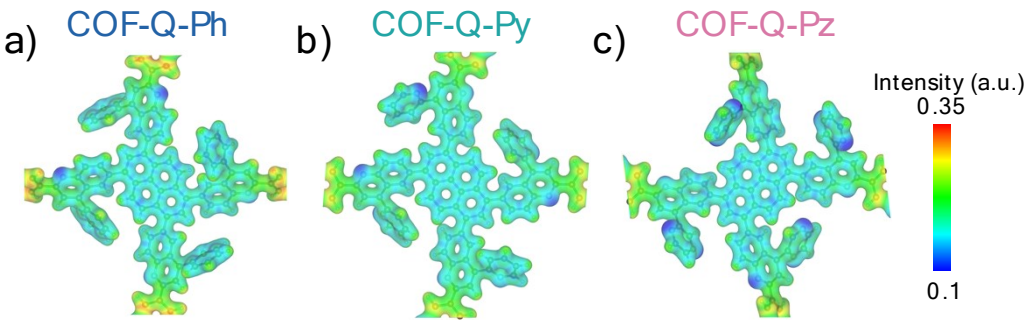

Fig. S33. Electrostatic potential maps of (a) COF-Q-Ph, (b) COF-Q-Py, and (c) COF-Q-Pz.

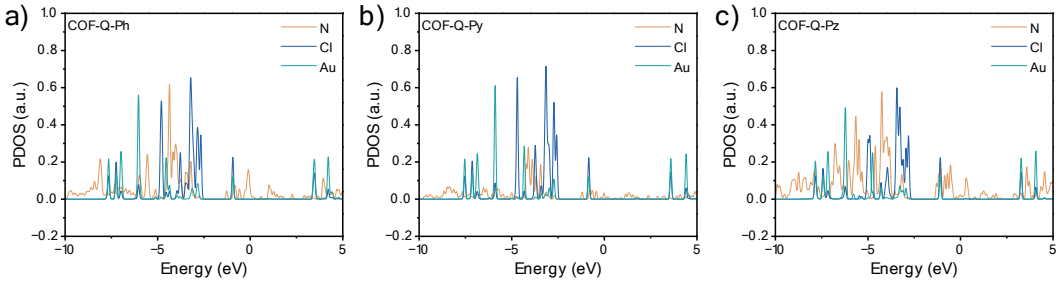

Fig. S34. Projected density of states (PDOS) of $AuCl_4^-$ adsorbed on COF-Q-Ph, COF-Q-Py, and COF-Q-Pz. (a–c) Element-resolved PDOS of N, Cl, and Au for the corresponding adsorption systems.

Table S1. Atomic coordinates for the unit cell of COF-Q-Ph.

Space group: P2/M a = b = 23.8149 Å, c = 3.4823 Å, α = β = γ = 90°							
Atom	X (Å)	Y (Å)	Z (Å)	Atom	X (Å)	Y (Å)	Z (Å)
C1	0.654672	10.70408	1.74115	N24	12.1818	20.15598	1.74115
C2	1.413652	11.85649	1.74115	C25	11.20896	21.08214	1.74115
C3	0.740405	13.05938	1.74115	C26	11.56475	22.48079	1.74115
C4	2.815874	11.82124	1.74115	C27	12.90887	22.86421	1.74115
N5	3.518651	12.95364	1.74115	C28	10.56619	23.4441	1.74115
C6	4.871576	12.98103	1.74115	C29	14.19535	12.92982	1.74115
C7	5.620316	11.80743	1.74115	C30	13.29586	13.95744	1.74115
C8	7.024443	11.90554	1.74115	C31	13.94553	3.115942	1.74115
C9	7.693403	13.11344	1.74115	C32	14.32014	4.436478	1.74115
C10	6.899653	14.2475	1.74115	C33	20.30054	13.1775	1.74115
C11	5.512673	14.18439	1.74115	C34	18.89284	13.22465	1.74115
C12	9.114915	13.23227	1.74115	C35	8.102543	19.08121	1.74115
C13	10.04441	12.1818	1.74115	C36	7.614338	17.79306	1.74115
C14	11.44282	12.43733	1.74115	C37	6.244267	17.52872	1.74115
C15	11.91721	13.74644	1.74115	C38	5.325964	18.55252	1.74115
C16	10.99605	14.80334	1.74115	C39	5.779876	19.83924	1.74115
C17	9.635509	14.49613	1.74115	C40	7.151138	20.09858	1.74115
C18	11.3347	16.15531	1.74115	C41	18.27341	14.4766	1.74115
C19	12.65619	16.6178	1.74115	C42	16.87714	14.63854	1.74115
C20	12.93316	17.95405	1.74115	C43	16.29106	15.87596	1.74115
C21	11.89149	18.86235	1.74115	C44	17.09553	16.98693	1.74115
C22	10.54548	18.4363	1.74115	C45	18.48393	16.85785	1.74115
C23	10.30542	17.09172	1.74115	C46	19.0643	15.61734	1.74115

Table S2. Atomic coordinates for the unit cell of COF-Q-Py.

Space group: P2/M a = 4.3550 Å, b = 3.4768 Å, c = 23.7619 Å, α = γ = 90°, β =87.7327°							
Atom	X (Å)	Y (Å)	Z (Å)	Atom	X (Å)	Y (Å)	Z (Å)
C1	-36.8112	-1.7384	24.46515	N24	-26.7273	-1.7384	35.83699
C2	-35.5896	-1.7384	25.15895	C25	-25.7718	-1.7384	34.87178
C3	-34.3969	-1.7384	24.41932	C26	-24.3435	-1.7384	35.24813
C4	-35.5516	-1.7384	26.56105	C27	-23.9728	-1.7384	36.59965
N5	-34.3576	-1.7384	27.20903	C28	-23.3398	-1.7384	34.26773
C6	-34.2677	-1.7384	28.56151	C29	-34.0725	-1.7384	37.87923
C7	-35.4364	-1.7384	29.36026	C30	-33.0382	-1.7384	36.96152
C8	-35.2781	-1.7384	30.75619	C31	27.9869	1.7384	13.96044
C9	-34.0169	-1.7384	31.37829	C32	29.33951	1.7384	14.33774
C10	-32.885	-1.7384	30.54083	C33	14.20597	1.7384	20.17432
C11	-33.0074	-1.7384	29.15416	C34	14.18668	1.7384	18.77032
C12	-33.8529	-1.7384	32.7963	C35	19.99609	1.7384	8.016065
C13	-34.9109	-1.7384	33.74963	C36	18.68303	1.7384	7.514824
C14	-34.6249	-1.7384	35.14081	C37	18.45345	1.7384	6.139556
C15	-33.277	-1.7384	35.58744	C38	19.53128	1.7384	5.257931
C16	-32.2089	-1.7384	34.6474	C39	20.8268	1.7384	5.771994
C17	-32.5445	-1.7384	33.28923	N40	21.02648	1.7384	7.117107
C18	-30.8212	-1.7384	34.97602	C41	39.79772	1.7384	18.10833
C19	-30.3463	-1.7384	36.29715	C42	39.91628	1.7384	16.7105
C20	-28.981	-1.7384	36.57876	C43	41.17413	1.7384	16.10811
C21	-28.0502	-1.7384	35.54066	C44	42.32008	1.7384	16.89903
C22	-28.4823	-1.7384	34.19365	C45	42.1843	1.7384	18.28594
C23	-29.8616	-1.7384	33.94694	N46	40.94688	1.7384	18.84986

Table S3. Atomic coordinates for the unit cell of COF-Q-Pz.

Space group: P2/M a = 24.3552 Å, b = 3.4738 Å, c = 23.7580 Å, α = γ = 90°, β =87.7327°							
Atom	X (Å)	Y (Å)	Z (Å)	Atom	X (Å)	Y (Å)	Z (Å)
C1	-36.7886	-1.7369	24.46337	N24	-26.6952	-1.7369	35.83201
C2	-35.5653	-1.7369	25.15396	C25	-25.7404	-1.7369	34.86604
C3	-34.3744	-1.7369	24.41162	C26	-24.312	-1.7369	35.2416
C4	-35.5239	-1.7369	26.55601	C27	-23.9411	-1.7369	36.59333
N5	-34.3282	-1.7369	27.20197	C28	-23.3092	-1.7369	34.26045
C6	-34.2361	-1.7369	28.55441	C29	-34.0424	-1.7369	37.87313
C7	-35.4036	-1.7369	29.35467	C30	-33.0071	-1.7369	36.95631
C8	-35.2446	-1.7369	30.75008	C31	27.99789	1.7369	13.95672
C9	-33.9836	-1.7369	31.37182	C32	29.35055	1.7369	14.33276
C10	-32.8519	-1.7369	30.53358	C33	14.21857	1.7369	20.16746
C11	-32.9751	-1.7369	29.14647	C34	14.1966	1.7369	18.76398
C12	-33.8202	-1.7369	32.79002	C35	20.00461	1.7369	8.017084
C13	-34.8787	-1.7369	33.74245	C36	18.6934	1.7369	7.512382
C14	-34.5936	-1.7369	35.13406	N37	18.47445	1.7369	6.172046
C15	-33.2457	-1.7369	35.58203	C38	19.50674	1.7369	5.291784
C16	-32.177	-1.7369	34.64242	C39	20.81363	1.7369	5.773222
C17	-32.5121	-1.7369	33.2838	N40	21.02945	1.7369	7.114507
C18	-30.7892	-1.7369	34.97121	C41	39.80542	1.7369	18.09832
C19	-30.314	-1.7369	36.29279	C42	39.92568	1.7369	16.70101
C20	-28.9488	-1.7369	36.57434	N43	41.15156	1.7369	16.11631
C21	-28.0182	-1.7369	35.53597	C44	42.28497	1.7369	16.86173
C22	-28.4508	-1.7369	34.18899	C45	42.18655	1.7369	18.25097
C23	-29.8295	-1.7369	33.94186	N46	40.95807	1.7369	18.8314

Table S4. Elemental analysis of COF-Q-Ph, COF-Q-Py, and COF-Q-Pz.

Sample	C (wt%)	H (wt%)	N (wt%)
COF-Q-Ph	85.42	4.75	4.92
COF-Q-Py	81.28	4.41	9.71
COF-Q-Pz	77.15	4.18	14.42

Table S5. Langmuir and Freundlich isotherm parameters for $AuCl_4^-$ adsorption on COF-Q-Ph, COF-Q-Py, and COF-Q-Pz.

	Langmuir			Freundlich		
	K_L (L/mg)	q_{max} (mg/g)	R^2	K_F $(mg/g)(L/mg)^{1/n}$	$1/n$	R^2
COF-Q-Ph	0.148	1263.1	0.999	395.9	0.227	0.839
COF-Q-Py	0.344	1814.3	0.996	625.8	0.245	0.778
COF-Q-Pz	0.366	2512.2	0.998	743.5	0.349	0.835

Table S6. Kinetic parameters for $AuCl_4^-$ adsorption on COF-Q-Ph, COF-Q-Py, and COF-Q-Pz based on pseudo-first-order and pseudo-second-order models.

	pseudo-first-order models		pseudo-second-order models	
	k_1 (min^{-1})	R^2	k_2 $(g \cdot mg^{-1} \cdot min^{-1})$	R^2
COF-Q-Ph	0.0334	0.977	1.44×10^{-4}	0.997
COF-Q-Py	0.0386	0.993	0.99×10^{-4}	0.999
COF-Q-Pz	0.0450	0.950	2.51×10^{-4}	0.998

Table S7. Thermodynamic parameters for $AuCl_4^-$ adsorption on COF-Q-Ph, COF-Q-Py, and COF-Q-Pz at different temperatures.

Adsorbent	T (K)	lnK_e	ΔG (kJ mol^{-1})	ΔH (kJ mol^{-1})	ΔS (J mol^{-1} K^{-1})
COF-Q-Ph	298	3.023	-7.48	14.05	72.26
	308	3.200	-8.21		
	318	3.380	-8.93		
COF-Q-Py	298	3.767	-9.31	31.56	137.14
	308	4.149	-10.68		
	318	4.569	-12.05		
COF-Q-Pz	298	4.521	-11.34	39.55	170.63
	308	5.162	-13.22		
	318	5.522	-14.75		

Table S8. Comparison of $AuCl_4^-$ adsorption performance of COF-Q-Pz with other reported adsorbents.

Adsorbent	pH	Equilibrium time (min)	q_{max} (mg/g)	Ref.
Tp-BDT-AA	5	360	3095	[1]
MTpPa-1	2	30	1737	[2]
COF-HNU25	7	8	1725	[3]
PAF-1-thiourea	5	120	2630	[4]
NH2-CTF-1	7.3	20	909	[5]
COF-TPTD-DHTA-TAB	5	300	2884	[6]
BTP-DET	2	250	2580.8	[7]
TTF-COF	4	240	2440	[8]
PYTA-PZDH-COF	7	240	2314	[9]
COF-2	3	480	2081	[10]
CF-COF	3	95	1895	[11]
im-PYTA-PZDH-COF	2	720	1558	[12]
isp^2c-COF_{ox}-NH_2	5	720	1389	[13]
COF-An	3	480	1080.7	[14]
DTDD-MOF	2	600	1119	[15]
UiO-66-BTU	4	240	680	[16]
TpDa-COF	4	360	983	[17]
COF-Q-Pz	3	40	2512.2	This work

References

1 S. Yang, T. Li, Y. Cheng, W. Fan, L. Wang, Y. Liu, L. Bian, C.-H. Zhou, L.-Y. Zheng and Q.-E. Cao, *ACS Sustainable Chem. Eng.*, 2022, **10**, 9719-9731.

2 Y. Bai, J. Yang, Q. Shuai and L. Huang, *Colloids Surf. A Physicochem. Eng. Asp.*, 2023, **657**, 130593.

3 J. Qiu, C. Xu, X. Xu, Y. Zhao, Y. Zhao, Y. Zhao and J. Wang, *Angew. Chem., Int. Ed.*, 2023, **62**, e202300459.

4 T. Ma, R. Zhao, Z. Li, X. Jing, M. Faheem, J. Song, Y. Tian, X. Lv, Q. Shu and G. Zhu, *ACS Appl. Mater. Interfaces*, 2020, **12**, 30474-30482.

5 H.-Y. Kong, Y. Tao, X. Ding and B.-H. Han, *Chem. Eng. J.*, 2023, **463**, 142393.

6 D. Mei and B. Yan, *ACS Mater. Lett.*, 2024, **7**, 220-228.

7 Y.-R. Chen, X.-Y. Fan, H.-F. Wei, L. Liao, Y. Hu, Y. Lu, X. Wang, Y. Li and W.-R. Cui, *Sep. Purif. Technol.*, 2024, **347**, 127521.

8 A. Zadehnazari, F. Auras, A. A. Altaf, A. Zarei, A. Khosropour, S. Amirjalayer and A. Abbaspourrad, *Nat. Commun.*, 2024, **15**, 10846.

9 X. Yang, D. Jiang, Y. Fu, X. Li, G. Liu, X. Ding, B. H. Han, Q. Xu and G. Zeng, *Small*, 2024, **20**, e2404192.

10 K. Li, D. Mei, Y.-s. Liu and B. Yan, *Chem. Mater.*, 2025, **37**, 2535-2545.

11 Q. Xu, X.-H. Du, D. Luo, M. Strømme, Q.-F. Zhang and C. Xu, *Chem. Eng. J.*, 2023, **458**, 141498.

12 B. Zhu, R. Luo, C. Hou, Y. Gao, Y. Zhang, K. Wang, L. Zhang and J. Luo, *Chem. Eng. J.*, 2024, **497**, 154885.

13 Y. Fan, W. Wang, A. Haleem, J. Pan and H. Li, *Sep. Purif. Technol.*, 2025, **353**, 128582.

14 L. Zhang, J.-Q. Fan, Q.-Q. Zheng, S.-J. Xiao, C.-R. Zhang, S.-M. Yi, X. Liu, W. Jiang, Q.-G. Tan, R.-P. Liang and J.-D. Qiu, *Chem. Eng. J.*, 2023, **454**, 140212.

15 Z. Huang, M. Zhao, C. Wang, S. Wang, L. Dai, L. Zhang and L. Xu, *Chem. Eng. J.*, 2020, **384**, 123343.

16 J. Guo, X. Fan, J. Wang, S. Yu, M. Laipan, X. Ren, C. Zhang, L. Zhang and Y. Li, *Chem. Eng. J.*, 2021, **425**, 130588.

17 D. Mei and B. Yan, *Angew. Chem., Int. Ed.*, 2024, **63**, e202402205.